A subgrid-scale estimation model applied to large eddy simulations of compressible turbulence

By J. A. Domaradzki[1], T. Dubois AND A. Honein

A subgrid-scale estimation procedure investigated previously for incompressible turbulence is extended to compressible flows. The procedure provides an estimate of the unfiltered velocity field and temperature appearing in the expressions for the subgrid-scale stress tensor and heat flux. The procedure in the physical space representation is applied to the compressible equations, which are written in a conservative form using sixth-order finite difference compact schemes for the approximation of the spatial derivatives. Two compressible flows are considered in this investigation: spatially decaying turbulence and shock/turbulence interaction. *A priori* analysis and actual large eddy simulations for both flows have been performed and a good agreement with filtered direct numerical simulations results has been obtained.

1. Introduction

Subgrid-scale (SGS) models commonly used in large eddy simulations (LES) of turbulent flows fall into three general categories: eddy viscosity models, similarity models, and so-called mixed models which combine eddy viscosity and similarity expressions. For review see Lesieur and Métais (1995) and Galperin and Orszag (1993). In recent years major advances in SGS modeling were made using the dynamic procedure (Germano *et al.* 1991, Lilly 1992, and Ghosal *et al.* 1995), which allows computation of model coefficients from a resolved LES field rather than prescribing them as constants. Despite evident progress in the field of SGS modeling, the existing models fail to capture some physical features of the actual SGS interactions. For instance, the eddy viscosity models properly model global SGS dissipation, *i.e.* the net energy flux from the resolved to the unresolved subgrid-scales, but predict very low correlations between the actual and modeled SGS quantities (Clark *et al.* 1979, Lund 1991, Kerr *et al.* 1996, O'Neil and Meneveau 1997). On the other hand, the similarity models correlate very well with the exact stresses in *a priori* analyses but significantly under predict SGS dissipation in actual large eddy simulations. Such difficulties motivate continuing search for better SGS models, and this effort is reflected in several articles in these Proceedings.

One such alternative approach to SGS modeling was proposed recently by Domaradzki *et al.* (1997, 1998). The proposed approach provides an estimate of the unfiltered velocity field appearing in the definition of the subgrid-scale stress tensor.

1 Department of Aerospace and Mechanical Engineering, University of Southern California, Los Angeles, California 90089-1191

Once the unfiltered velocity is found, it is used to compute all SGS quantities directly from the definitions. The estimation model was implemented and evaluated for incompressible channel flow at low and moderate Reynolds numbers, providing very good agreement with the DNS and experimental results. However, further work is needed to evaluate, document, and improve the performance of the model for higher Reynolds numbers and different flows. In this report we extend the SGS estimation model to compressible flows and evaluate its performance for spatially decaying compressible turbulence and shock/turbulence interaction.

2. Formulation

2.1 The large eddy simulation equations

The LES equations are obtained by spatial filtering of Navier-Stokes equations for compressible flows. The result is rewritten in terms of Favre (or density-weighted) filtering, which for a function f is defined as

$$\tilde{f} = \frac{\overline{\rho f}}{\bar{\rho}},$$

where the overbar denotes spatial filtering with a top-hat filter with the filter width Δ_f and ρ is the density. We follow Moin *et al.* (1991) and Erlebacher *et al.* (1992) in neglecting several terms in the equations that are considered small. Resulting continuity and momentum equations for spatially filtered density $\bar{\rho}$ and Favre filtered velocity $\tilde{u}_i$ are

$$\frac{\partial \bar{\rho}}{\partial t} + \frac{\partial}{\partial x_i}(\bar{\rho}\tilde{u}_i) = 0, \tag{1a}$$

$$\frac{\partial \bar{\rho}\tilde{u}_i}{\partial t} + \frac{\partial}{\partial x_j}\left(\bar{\rho}\tilde{u}_i\tilde{u}_j + \bar{p}\delta_{ij}\right) = \frac{\partial \tilde{\sigma}_{ij}}{\partial x_j} - \frac{\partial \tau_{ij}}{\partial x_j}. \tag{1b}$$

In Eq. (1) $\tilde{\sigma}_{ij}$ is the viscous stress, that is

$$\tilde{\sigma}_{ij} = \overline{\mu}\left(\frac{\partial \tilde{u}_i}{\partial x_j} + \frac{\partial \tilde{u}_j}{\partial x_i} - \frac{2}{3}\frac{\partial \tilde{u}_k}{\partial x_k}\delta_{ij}\right), \tag{2}$$

where μ is the viscosity and τ_{ij} represents the subgrid-scale (SGS) stress,

$$\tau_{ij} \;=\; \bar{\rho}(\widetilde{u_i u_j} - \tilde{u}_i\tilde{u}_j) = \overline{\rho u_i u_j} - \overline{\rho u_i}\;\overline{\rho u_j}/\bar{\rho}. \tag{3}$$

According to Lee (1992), a conservative formulation for the energy equation is required in the computation of shock/turbulence interaction. Following Mahesh (1998), the conservative energy equation is written as,

$$\frac{\partial E_T}{\partial t} + \frac{\partial}{\partial x_i}\left[(E_T + p)u_i\right] \;=\; \frac{\partial}{\partial x_j}(u_i\sigma_{ij}) - \frac{\partial}{\partial x_i}\left(\kappa\frac{\partial T}{\partial x_i}\right), \tag{4}$$

where the total energy is given by $E_T = \rho C_v T + \rho u_k u_k/2$, κ is the thermal conductivity, and C_v is the specific heat at constant volume.

Using the definition of the Favre filtering and of the total energy, the term $\overline{E_T u_i}$ in (4) can be rewritten as

$$\begin{aligned}\overline{E_T u_i} &= \bar{\rho} C_v \tilde{T} \tilde{u}_i + C_v q_i + \frac{1}{2}\bar{\rho}\widetilde{u_k u_k u_i} \tilde{u}_i + \frac{1}{2}\bar{\rho}\left(\widetilde{u_k u_k u_i} - \widetilde{u_k u_k}\tilde{u}_i\right) \\ &= \bar{E}_T \tilde{u}_i + C_v q_i + \frac{1}{2}\bar{\rho}\left(\widetilde{u_k u_k u_i} - \widetilde{u_k u_k}\tilde{u}_i\right),\end{aligned} \tag{5}$$

where the subgrid-scale heat flux q_i is

$$q_i = \bar{\rho}\left(\widetilde{T u_i} - \tilde{T}\tilde{u}_i\right) = \overline{\rho u_i T} - \overline{\rho u_i}\,\overline{\rho T}/\bar{\rho} \tag{6}$$

The last term in (5), corresponding to convection of SGS kinetic energy by SGS velocity, is expected to be small and is neglected. The other nonlinear term on the left-hand side of (4), involving pu_i, is rewritten after filtering as follows,

$$\overline{pu_i} \;=\; \overline{\rho R T u_i} \;=\; \bar{\rho} R \widetilde{T u_i} \;=\; \bar{\rho} R \tilde{T}\tilde{u}_i + R q_i,$$

In the last formula the equation of state for ideal gas $p = \rho R T$ was used, where R is the gas constant. The filtered r.h.s. of Eq. (4) is treated as in Moin *et al.* (1991), leading to the final form of the filtered total energy equation

$$\begin{aligned}\frac{\partial \bar{E}_T}{\partial t} + \frac{\partial}{\partial x_i}\left((\bar{E}_T + \bar{\rho} R \tilde{T})\tilde{u}_i\right) = &-\frac{\partial}{\partial x_i}\left(C_p q_i\right) \\ &+ \frac{\partial}{\partial x_i}\left(\overline{\kappa}\frac{\partial \tilde{T}}{\partial x_i}\right) + \frac{\partial}{\partial x_i}\left(\tilde{\sigma}_{ij}\tilde{u}_i\right).\end{aligned} \tag{7}$$

In deriving (7) the filtered equation of state was used, $\overline{p} = \bar{\rho} R \tilde{T}$, and the relation $C_p = C_v + R$, where C_p is the specific heat at constant pressure. Finally, note that the resolved temperature and total energy are related by

$$\bar{E}_T \;=\; \bar{\rho} C_v \tilde{T} + \frac{1}{2}\bar{\rho}\tilde{u}_k\tilde{u}_k + \frac{1}{2}\tau_{kk}. \tag{8}$$

To close the above equations for the primitive variables $\overline{\rho}, \tilde{u}_i, \tilde{T}$, the SGS stress (3) and the SGS heat flux (6) must be expressed in terms of those variables using an SGS model.

2.2 The subgrid scale estimation procedure

Consider a velocity field u_i which is a continuous function of variable x on the interval $[0, L_x]$. For the purpose of numerical simulations, u_i may be approximated in terms of its values at discrete points using sufficiently small mesh size Δ_{DNS}. Assume that the continuous function u_i is filtered with a top hat filter Δ_f. In general, the filtered velocity $\overline{u}_i$ is smoother than the unfiltered field u_i, and it can

be accurately represented by sampling it on a coarser mesh $\Delta_{LES} \approx \Delta_f \ll \Delta_{DNS}$. Specifically, we will choose $\Delta_{LES} = \Delta_f/2$.

The SGS estimation procedure consists of two steps. In the kinematic step we seek a function $u_i^0(x)$ such that

$$\overline{u_i^0}(x_n) = \overline{u}_i(x_n), \tag{9}$$

on the LES mesh points $x_n = n\Delta_{LES},\ (n = 0, 1, \ldots, N)$. Note that the right-hand side of Eq. (9) are the values of the resolved field, assumed to be known on the LES mesh. Clearly, without additional assumptions the above condition does not provide a unique solution for $u_i^0(x)$. To further specify the problem we assume that $u_i^0(x)$ may be accurately represented by N nodal values, $u_i^0(x_n)$. Then, the filtering on the left-hand side of Eq. (9) involves integration over interval Δ_f spanning three neighboring points. We use the Simpson's rule for the integration, which results in a tridiagonal system of equations for the values of $u_i^0(x_n)$

$$\frac{1}{6}\left[u_i^0(x_{n-1}) + 4u_i^0(x_n) + u_i^0(x_{n+1})\right] = \overline{u}_i^{(N)}(x_n). \tag{10}$$

The system can be solved if values for the end points are provided. In this work we apply the procedure to periodic functions only.

The subgrid scales are generated in the nonlinear step on a fine mesh with the mesh size $\Delta_{LES}/2$

$$x_j = j\Delta_{LES}/2,\ (j = 0, 1, \ldots, 2N). \tag{11}$$

First, we interpolate previously computed u_j^0 from the coarse LES mesh to the fine mesh using cubic splines. Next, the small scales are produced as a result of nonlinear interactions among large scales. To this end the advection effects by the large scales are removed from the nonlinear term

$$N_i^0 = -(u_j^0 - \overline{u_j^0})\frac{\partial}{\partial x_j}u_i^0, \tag{12}$$

and the growth rate of subgrid scales by the nonlinear interactions among resolved scales is obtained as

$$N_i' = N_i^0 - \overline{N_i^0}. \tag{13}$$

If the nonlinear interactions are maintained over time θ, the small scales become

$$u_i' = \theta N_i', \tag{14}$$

and the estimated velocity field is

$$u_i^e = u_i^0 + u_i'. \tag{15}$$

To fully determine the small scales using the nonlinear correction term Eq. (14), the time scale θ is needed. Physically θ can be interpreted as the large eddy turnover

time. Its value may vary with the position in a flow to reflect local conditions of turbulence. We estimate θ, assuming that locally in space the energy of subgrid scales Eq. (14) is proportional to the energy of the smallest resolved scales. This provides the following expression

$$\theta = C\sqrt{\frac{(u_i^0 - \overline{u_i^0})^2}{N_i'^2}}, \tag{16}$$

where the constant of proportionality C is found to be approximately $1/2$ for the inertial range spectral form.

For applications to compressible flows the following changes are made. First, the deconvolution for ρ is performed providing unfiltered ρ^0. To avoid violating the conservation of mass, no attempt is made to use the nonlinear correction for SGS density scales. Next the deconvolution is performed for spatially filtered velocities, $\overline{\rho u_i} = \bar{\rho}\tilde{u}_i$. The resulting quantities are divided by ρ^0 to provide u_i^0 for use in the nonlinear correction step as described above. Similarly, the deconvolution for $\overline{E}_T$ is performed, and the relation for E_T^0 in terms of ρ^0, u_i^0, and T^0 is solved for the temperature T^0. The nonlinear correction to T^0 is found as for the velocity by replacing the nonlinear term for the velocity by the nonlinear term for the temperature. Estimated density $\rho^e = \rho^0$, velocity $u_i^e = u_i^0 + u_i'$, and temperature $T^e = T^0 + T'$ are used to calculate the SGS stress and the SGS heat flux from formulas (3) and (6), respectively.

3. Numerical implementation

Two test cases have been considered, namely spatially decaying turbulence and the interaction of isotropic turbulence with a shock wave. For both cases, DNS data are available and were used for *a priori* tests and comparisons with large eddy simulations. The DNS code uses modified sixth-order Padé (compact) scheme for discretization of the spatial derivatives and a third order (low storage) Runge-Kutta scheme for the time discretization. In the shock/turbulence interaction case, a sixth-order ENO scheme is used in the vicinity of the shock wave, i.e. $x \simeq 2$; it is applied only in the streamwise (shock-normal) direction.

The cubic computational domain has dimensions L_x, L_y, and L_z in three Cartesian directions. The grid points are clustered around the shock in the streamwise direction while a uniform mesh is used in the cross-stream directions y and z. Approximately non-reflecting boundary conditions are specified at the exit, i.e. $x \simeq L_x$. In the cross-stream directions periodic boundary conditions are imposed. The mean flow is in the x direction. In spatial simulation, a uniform mesh is used in all spatial directions. Moreover, the flow is supersonic so that the primitive variables are specified at the inflow boundary $x = 0$ and no boundary conditions are needed at the outflow $x = L_x$.

The generation of inflow conditions is described in Mahesh *et al.* (1996). First, a temporal (decaying) simulation of isotropic turbulence is conducted. The resolution and domain size are the same as used for the spatial simulation and are listed in

Table 1. The Reynolds number based on the Taylor microscale and the turbulent Mach number at the initial time are $Re_\lambda = 30$ and $M_t = 0.17$, respectively. The simulation is advanced until a state of fully developed turbulence is reached. Turbulent fluctuations obtained in such a simulation are then superimposed on spatially uniform mean values of the velocity, pressure, and density at the inflow. Inflow turbulence is advected through the computational domain by the mean velocity and decays with the increasing distance from the inflow plane.

The estimation model was implemented only in the cross-stream directions y and z, and the full DNS resolution was used in the streamwise x direction. Parameters for all simulated cases are summarized in Table 1 for the spatial simulations (prefix SP) and in Table 2 for the shock/turbulence interaction case (prefix SH). For both flows *a priori* tests were performed using high resolution DNS databases hiDNS. After that the model was implemented in time evolving large eddy simulations, cases SPLES-1 and SHLES-1, for the respective spanwise resolutions in each direction a factor of three and four less than the full DNS resolution. Additionally, for the compressible turbulence case a simulation without a model was performed (case SPloDNS) with the same low resolution as the case SPLES-1. Comparing these two cases allows assessment of the relative importance of the model in the flow evolution.

Table 1. Parameters of the spatially decaying turbulence.

Case	Grid	$L_x \times L_y \times L_z$	Re_λ	M_t
SPhiDNS	$97 \times 97 \times 97$	$2\pi \times 2\pi \times 2\pi$	30	0.17
SPloDNS	$97 \times 33 \times 33$	$2\pi \times 2\pi \times 2\pi$	30	0.17
SPLES-1	$97 \times 33 \times 33$	$2\pi \times 2\pi \times 2\pi$	30	0.17

Table 2. Parameters of the simulations of shock/turbulence interaction.

Case	Grid	$L_x \times L_y \times L_z$	Re_λ	M	M_t
SHhiDNS	$231 \times 81 \times 81$	$10 \times 2\pi \times 2\pi$	19.1	1.29	0.14
SHLES-1	$231 \times 21 \times 21$	$10 \times 2\pi \times 2\pi$	19.1	1.29	0.14

A number of physical quantities are available from the numerical simulation results. In addition to SGS stress (3) and SGS heat flux (6), an important quantity is the SGS dissipation per unit mass

$$\epsilon_{SGS} = \frac{1}{\bar{\rho}} \tau_{ij} \frac{\partial \tilde{u}_i}{\partial x_j}, \tag{17}$$

which affects the resolved kinetic energy $K = \frac{1}{2}\tilde{u}_i\tilde{u}_i$. The SGS kinetic energy is $K_{SGS} = \frac{1}{2}(u_i u_i - \tilde{u}_i\tilde{u}_i)$. For plotting purposes all computed fields are reduced

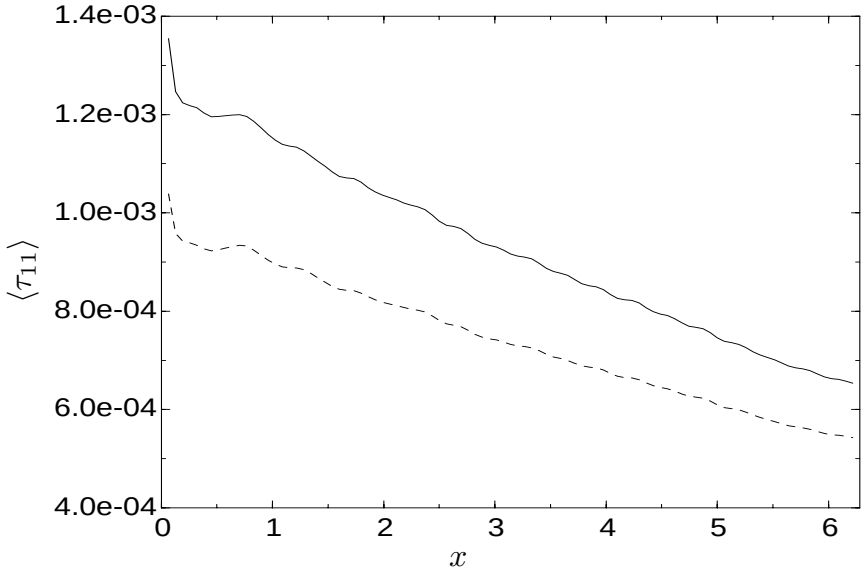

FIGURE 1. The plane average component of the streamwise component of the SGS stress tensor $\langle\tau_{11}\rangle$. ——— : case SPhiDNS; ------ : value predicted by the estimation procedure.

to functions of the streamwise variable x by averaging over spanwise planes and over several realizations. Such averages are signified by brackets $< ... >$. To assess predictions of the backscatter by the model, the SGS dissipation is decomposed in each cross-stream plane into forward transfer (negative values, $< \epsilon^{-}_{SGS} >=< (\epsilon_{SGS} - |\epsilon_{SGS}|)/2 >$) and inverse transfer or backscatter (positive values, $< \epsilon^{+}_{SGS} >=< (\epsilon_{SGS} + |\epsilon_{SGS}|)/2 >$).

3.1 Spatially decaying turbulence

In *a priori* tests the exact SGS quantities computed from the fully resolved DNS fields were compared with the SGS quantities predicted by the estimation model. Spanwise resolution was reduced from 97×97 mesh points in DNS to 33×33 points for the model. Calculated correlation coefficients between the exact and the modeled SGS quantities were found to always exceed 90%. These values are much higher than for the eddy viscosity based models and comparable to values observed for the similarity models.

In Fig. 1 we plot the averaged τ_{11} component of the SGS stress tensor computed exactly and using the estimation model. The error in the model prediction is about 25% at the inflow, decreasing to 15% at the outflow. It is well known that a success of a SGS model critically depends on its ability to correctly predict the SGS dissipation. In Fig. 2 we plot the actual and the model SGS dissipation decomposed into forward transfer (negative curves) and backscatter (positive curves). The agreement between the exact and the modeled quantities is now much better than for the SGS stresses. However, the forward transfer is slightly under predicted by the model. This may be a cause for concern because even small errors in the SGS dissipation may accumulate in actual LES, leading to incorrect long time dynamics. This is the problem commonly encountered by pure similarity models. In order to fully

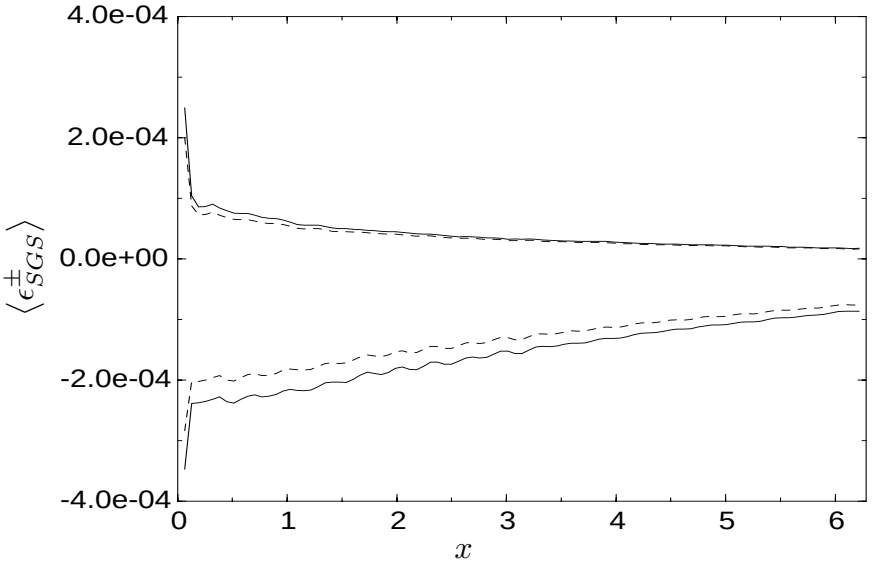

FIGURE 2. Negative and positive values of local SGS dissipation averaged over the cross-stream directions $\langle \epsilon^{\pm}_{SGS} \rangle$. ——— : case SPhiDNS; ------ : value predicted by the estimation procedure.

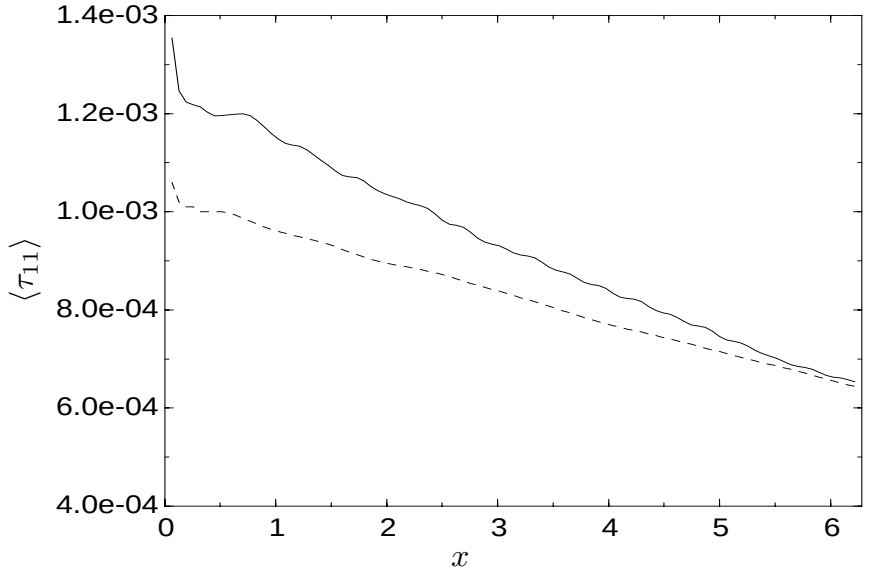

FIGURE 3. The plane averaged component of the streamwise component of the SGS stress tensor $\langle \tau_{11} \rangle$. ——— : case SPhiDNS; ------ : case SPLES-1.

assess a SGS model, actual LES must be performed over sufficiently long evolution times. Such LES with the estimation model have been performed, and the results are reported below.

In Fig. 3 we compare the exact value of τ_{11} component of the SGS stress tensor with the value it has in the well developed large eddy simulation run SPLES-1. It is interesting to note that the agreement is now better than in *a priori* test. We offer the following explanation. If SGS quantities are under predicted by the model at

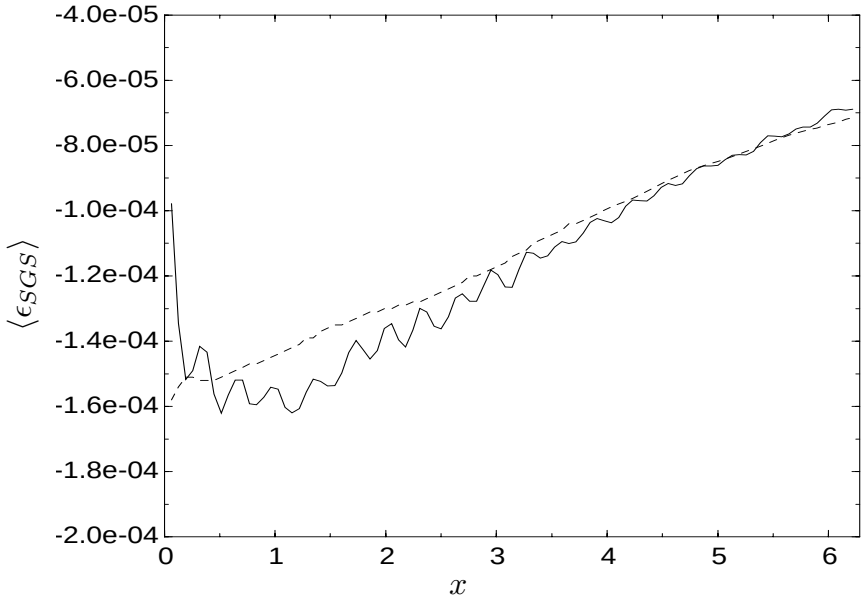

FIGURE 4. The plane averaged SGS dissipation $\langle \epsilon_{SGS} \rangle$. ——— : case SPhiDNS; ------ : case SPLES-1.

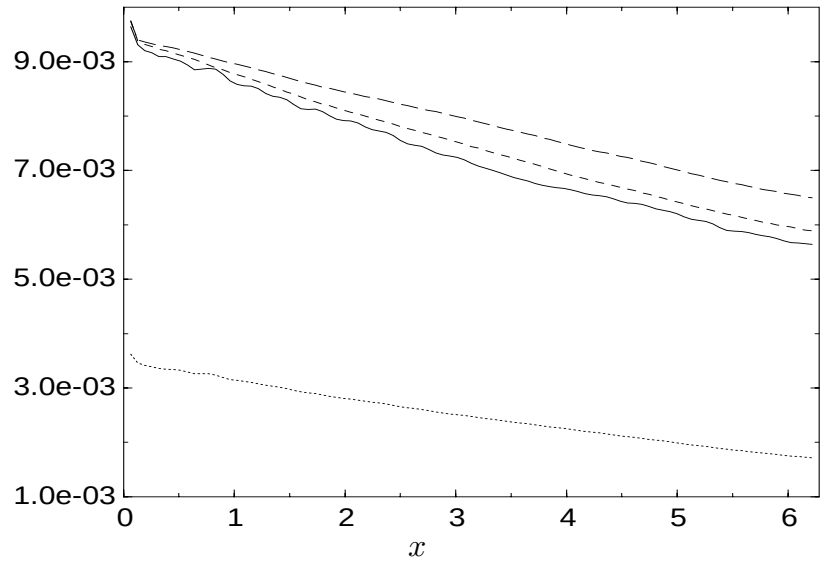

FIGURE 5. Plane averaged resolved kinetic energy $\frac{1}{2}\langle \bar{u}_i \bar{u}_i \rangle$. ——— : case SPhiDNS; ------ : case SPLES-1; – – – – : case SPloDNS; ····· : SGS kinetic energy $\frac{1}{2}\langle u_i u_i - \bar{u}_i \bar{u}_i \rangle$.

the initial time, the energy levels of the resolved scales will start increasing in the simulations. Because of the dependence of the estimation procedure on the resolved scales, this will lead to the increase of the SGS quantities until a balance is reached.

The total SGS dissipation for the run SPLES-1 averaged over time is plotted in Fig. 4 where it is compared with the exact SGS dissipation in the run SPhiDNS. There is more variability present in the DNS results because fewer fields were available for time averaging than for the LES run. The model appears to slightly under

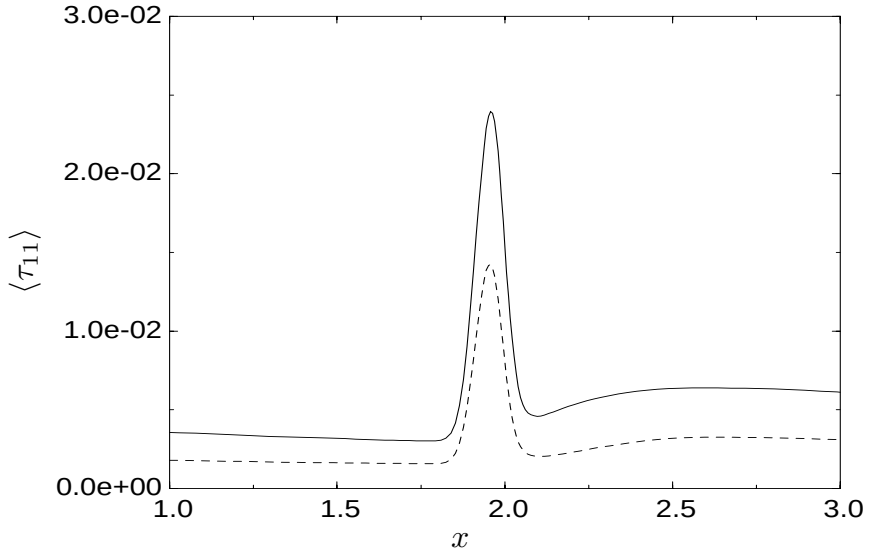

FIGURE 6. The plane averaged component of the streamwise component of the SGS stress tensor $\langle \tau_{11} \rangle$. ——— : case SHhiDNS; ------ : value predicted by the estimation procedure.

predict the exact quantity in the vicinity of the inlet $x < 2$, but the prediction becomes progressively better as the flow evolves away from the inlet. These results are entirely consistent with the results of the *a priori* analysis. We thus conclude that the estimation model maintains correct levels of the SGS dissipation in the actual LES. This feature clearly differentiates it from the classical similarity models. It should also allow proper prediction of the evolution of the turbulent kinetic energy.

In Fig. 5 we plot the dependence of the kinetic energy on the streamwise distance from the inlet. The resolved kinetic energy in LES decays somewhat more slowly than the corresponding quantity obtained from high resolution DNS, consistent with the under prediction of the SGS dissipation by the estimation model in run SPLES-1. However, if no model is used the energy prediction deteriorates markedly (case SPloDNS), indicating that the estimation model has a significant effect on the simulations. This conclusion is further confirmed by noting that in the simulation the SGS kinetic energy is not negligible and constitutes about 25% of the total kinetic energy in DNS.

3.2 Shock/turbulence interaction

For the shock/turbulence interaction problem, the low spanwise resolution of 21×21 mesh points provides a more severe test of the model since a run without the model at this resolution quickly became unstable. All SGS quantities for this problem have much larger values in the vicinity of the shock location $x = 2$ than away from the shock, and that region is emphasized in the plots. In Figs. 6, 7, and 8 we compare the exact and modeled SGS stress component τ_{11}, SGS heat flux q_1, and SGS dissipation ϵ_{SGS}, respectively, obtained in *a priori* analysis. We observe that all SGS quantities are predicted in a qualitative agreement with the exact data, in particular the peak locations, but the model values are not quantitatively

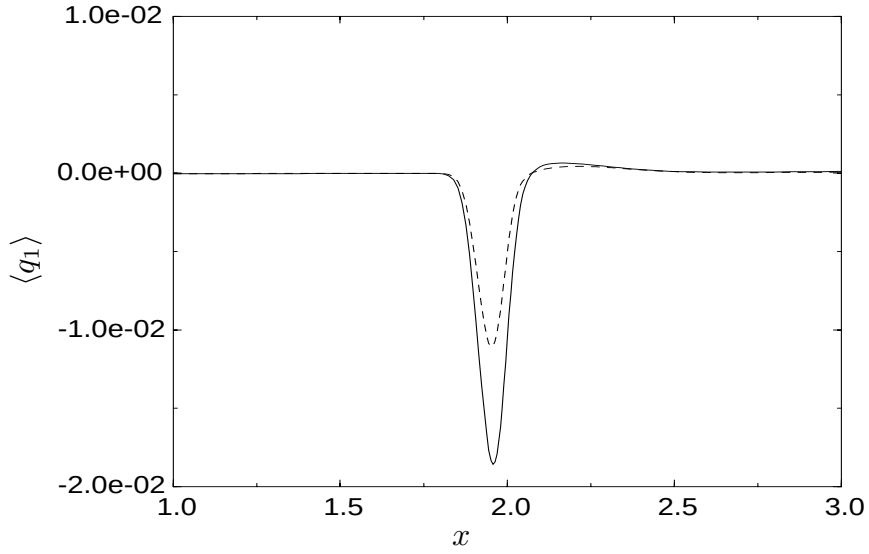

FIGURE 7. The plane averaged component of the streamwise component of the SGS heat flux $\langle q_1 \rangle$. ——— : case SHDNS; ------ : value predicted by the estimation procedure.

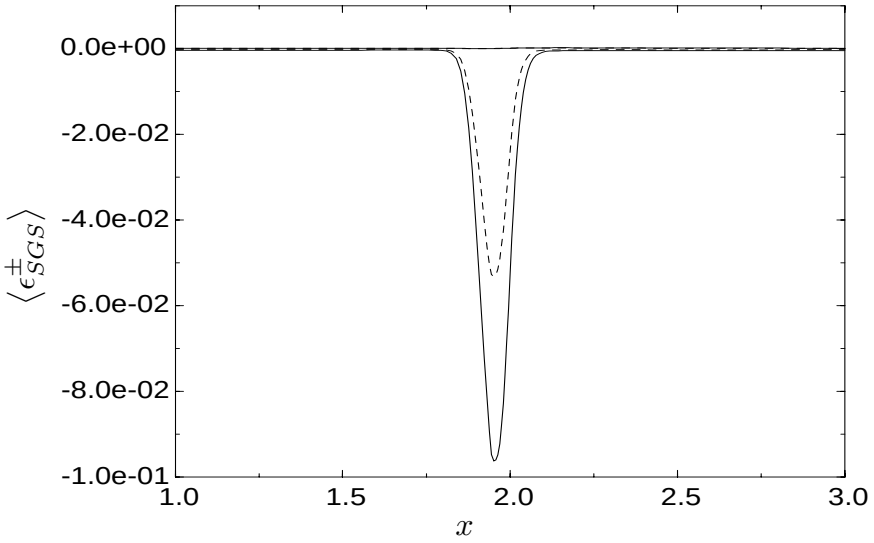

FIGURE 8. Negative and positive values of local SGS dissipation averaged over the cross-stream directions $\langle \epsilon^{\pm}_{SGS} \rangle$. ——— : case SHDNS; ------ : value predicted by the estimation procedure.

accurate. We also find that for this problem the backscatter component of the SGS dissipation is negligible compared with the forward transfer (Fig. 8). When the estimation model is implemented in time evolving LES, the agreement between the LES and exact SGS data improves. This is illustrated in Figs. 9 - 11 and is consistent with the similar behavior observed for the decaying turbulence case.

While good predictions of SGS quantities are an important test of an SGS model,

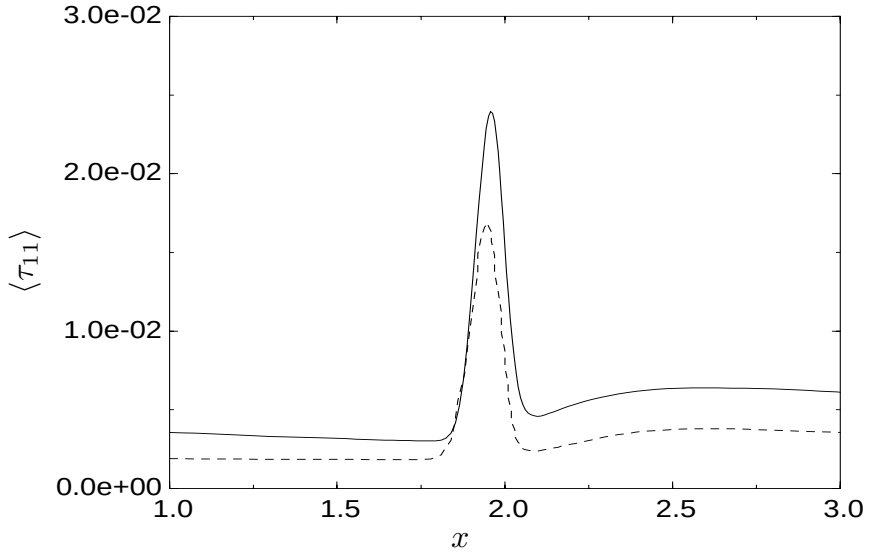

FIGURE 9. The plane averaged component of the streamwise component of the SGS stress tensor $\langle \tau_{11} \rangle$. ——— : case SHhiDNS; ------ : case SHLES-1.

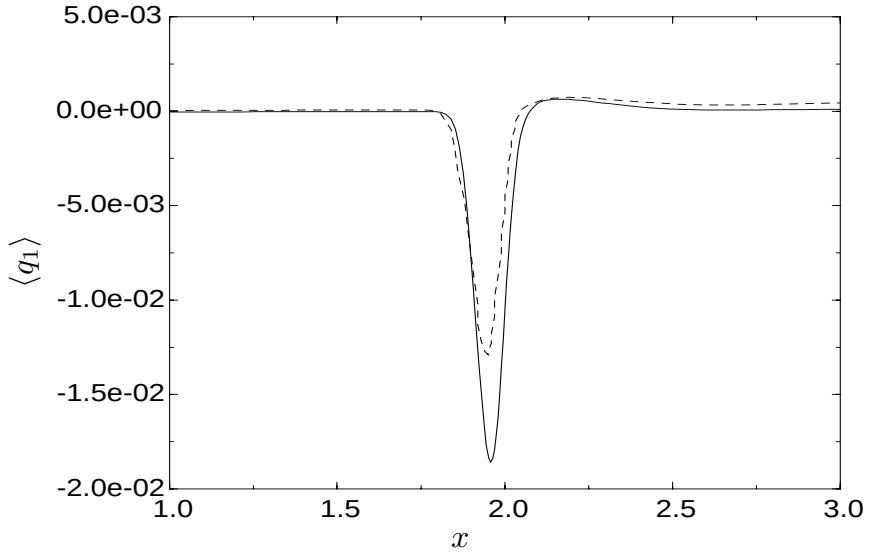

FIGURE 10. The plane averaged component of the streamwise component of the SGS heat flux $\langle q_1 \rangle$. ——— : case SHhiDNS; ------ : case SHLES-1.

the LES practice is concerned with predictions of physical quantities that are accessible to experimental measurements. Two such quantities are the turbulent kinetic energy and the mean velocity. In Fig. 12 we compare the mean velocity obtained in the LES case SHLES-1 with the mean velocity for the case SHhiDNS. The comparison is very good though the location of the shock in LES is slightly shifted upstream. A similar shift is observed for the kinetic energy in Fig. 13 (see the inset). The resolved energy decays before and after the shock, and the estimation model is clearly capable of capturing that decay though it over estimates the energy levels in those regions. In the shock region, magnified in the inset, the energy levels

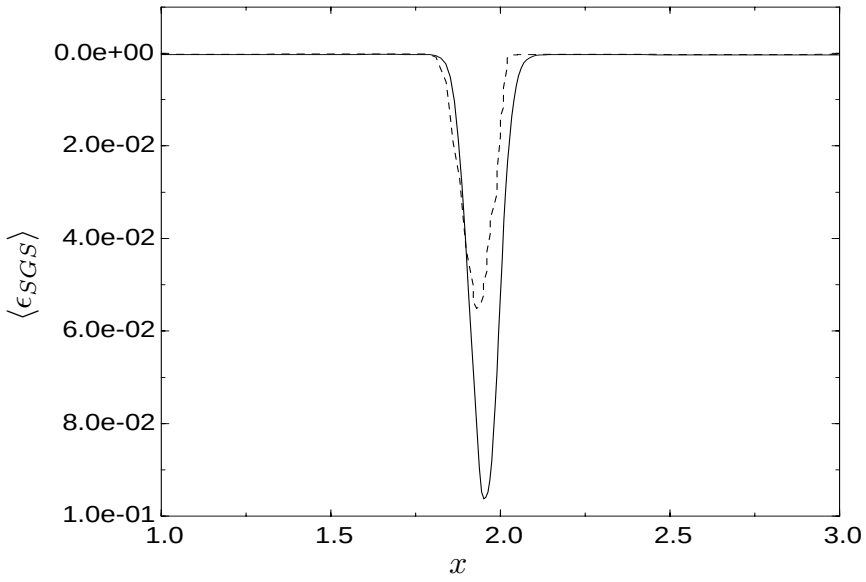

FIGURE 11. Plane averaged SGS dissipation: $\langle \epsilon_{SGS} \rangle$. ——— : case SHhiDNS; ------ : case SHLES-1.

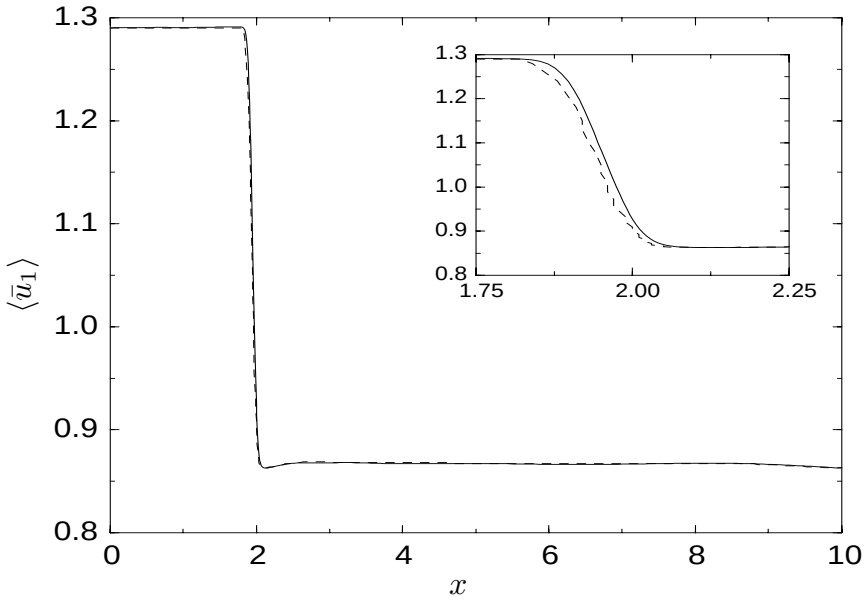

FIGURE 12. Mean velocity profile $\langle \bar{u}_1 \rangle$. ——— : case SHhiDNS; ------ : case SHLES-1.

in LES are in excellent agreement with the resolved energy in DNS. Overall, for all x the SGS energy component is of the same order as the resolved energy, pointing to a significant effect of the model on the LES. Similar behavior was observed for other LES quantities such as density, pressure, and temperature, i.e. uniformly good agreement with the DNS results and a slight upstream shift of the LES curves with respect to the DNS curves.

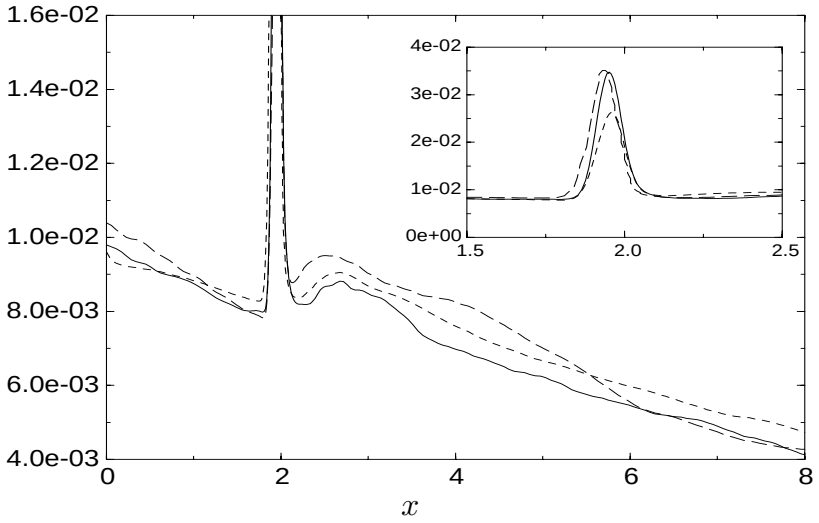

FIGURE 13. Plane averaged resolved kinetic energy $\frac{1}{2}\langle \bar{u}_i \bar{u}_i \rangle$. ——— : case SHhiDNS; – – – – : case SHLES-1; - - - - - - : plane averaged SGS kinetic energy $\frac{1}{2}\langle u_i u_i - \bar{u}_i \bar{u}_i \rangle$.

4. Conclusions

The subgrid-scale estimation model developed previously for incompressible flows was extended to compressible turbulence. The basic modeling principle is to recover unfiltered, resolved scales from a filtered LES field using the deconvolution procedure and to generate a range of smaller subgrid-scales through nonlinear interactions among resolved ones. In principle, the technique should be applicable to filtered evolution equations for any system whose dynamics are governed by nonlinear interactions which produce local energy cascade. In compressible turbulence both the velocity and temperature (or energy) dynamics have this property. Consequently, the estimation procedure used for incompressible turbulence could be applied with only minor modifications to the velocity and temperature fields in compressible turbulence. The performance of the estimation procedure was evaluated by comparing model results with high resolution DNS databases for two flows: spatially decaying compressible turbulence and shock/turbulence interaction. In both cases SGS quantities obtained using the estimation model showed high correlations with the exact DNS results in *a priori* tests. However, the values of the modeled quantities were generally less than the exact values. This feature of *a priori* tests indicates that either the modeled SGS scales do not provide a perfect approximation to the actual SGS scales or that more nonlocal interactions than accounted for by the model should be included. At low Reynolds numbers considered here, the latter explanation is unlikely. Therefore, we believe that further work on improving the quality of the estimated SGS scales is needed. Deficiencies of the modeled scales had negligible effect on the quality of the results in actual LES, which showed much better agreement with the DNS results than *a priori* tests. This was explained by the dynamic coupling between the model and the resolved scales, which in the time evolving LES increases the SGS quantities over their *a priori* values.

Overall, the results presented in this report strongly support the claim that the estimation model accounts properly for the SGS interactions in compressible turbulence. However, it must be noted that only low Reynolds number flows were considered. We cannot exclude a possibility that any deficiencies of the estimated scales, which did not appear to be significant at low Reynolds numbers, will become amplified at high Reynolds numbers. Also, neglecting the nonlocal transfers may no longer be a valid approximation at high Reynolds numbers. The former deficiencies would need to be corrected by developing better approximations to the subgrid scales at high Reynolds numbers while the latter effects are amenable to eddy viscosity modeling. Moreover, because of the particular geometry for both problems, the model could be applied only in two cross-stream directions. For more general problems, e.g. flows with more complex shock patterns, the model will have to be applied in all three spatial directions. An extension of the procedure to incorporate filtering in all three directions is straigthforward and is currently being tested on the channel flow problem.

Acknowledgments

JAD was partially supported by the NSF Grant CTS-9704728, and by CTR.

REFERENCES

Clark, R. A. & Ferziger J. H. & Reynolds, W. C. 1979 Evaluation of subgrid-scale models using an accurately simulated turbulent flow. *J. Fluid Mech.* **91,** 1.

Domaradzki, J. A. & Saiki, E. M. 1997 A subgrid-scale model based on the estimation of unresolved scales of turbulence. *Phys. Fluids.* **9**(7)**,** 2148-2164.

Domaradzki, J. A. & Loh, K. 1998 The subgrid-scale estimation model in the physical space representation. *Phys. Fluids.* (Submitted)**.**

Erlebacher, G. & Hussaini, M. Y. & Speziale, C. G. & Zang, T. A. 1992 Toward the large-eddy simulation of compressible turbulent flows. *J. Fluid Mech.* **238,** 155-185.

Galperin, B. & Orszag, S. A. eds. 1993 Large eddy simulation of complex engineering and geophysical flows. Cambridge University Press, Cambridge.

Germano, M. & Piomelli, U. & Moin, P. & Cabot, W. H. 1991 A dynamic subgrid-scale eddy viscosity model. *Phys. Fluids A.* **3**(7)**,** 1760-1765.

Ghosal, S. & Lund, T. S. & Moin, P. & Akselvoll, K. 1995 A dynamic localization model for large-eddy simulation of turbulent flows. *J. Fluid Mech.* **286,** 229-255.

Kerr, R. M. & Domaradzki, J. A. & Barbier, G. 1996 Small-scale properties of nonlinear interactions and subgrid-scale energy transfer in isotropic turbulence. *Phys. Fluids.* **8,** 197.

Lee, S. 1992 Large eddy simulation of shock turbulence interaction. *Annual Research Briefs.* Center for Turbulence Research, NASA Ames/Stanford Univ., 73-84.

Lesieur, M. & Métais, O. 1996 New trends in large-eddy simulations of turbulence. *Ann. Rev. Fluid Mech.* **28,** 45.

Lilly, D. K. 1992 A proposed modification of the Germano subgrid-scale closure method. *Phys. Fluids A.* **4**(3)**,** 633-635.

Lund, T. S. 1991 On dynamic models for large eddy simulations. *Annual Research Briefs.* Center for Turbulence Research, NASA Ames/Stanford Univ., 177-190.

Mahesh, K. 1998 Private communication.

Mahesh, K. & Lele, S. K. & Moin, P. 1997 The influence of entropy fluctuations on the interaction of turbulence with a shock wave. *J. Fluid Mech.* **334,** 353-379.

Moin, P. & Squires, K. & Cabot, W. & Lee, S. 1991 A dynamic subgrid-scale model for compressible turbulence and scalar transport. *Phys. Fluids A.* **3**(11)**,** 2746-2757.

O'Neil, J. & Meneveau, C. 1997 Subgrid-scale stresses and their modeling in a turbulent wake. *J. Fluid Mech.* **349,** 253.